Manual on Experimental Stress Analysis

Fifth Edition

James F. Doyle and
James W. Phillips, eds.

Society for Experimental Mechanics

6. PHOTOELASTICITY

Daniel Post[1]

6. 1. INTRODUCTION

Photoelasticity is an experimental technique for stress and strain analysis that is particularly useful for members having complicated geometry, complicated loading conditions, or both. For such cases, analytical methods (that is, strictly mathematical methods) may be cumbersome or impossible, and analysis by an experimental approach maybe more appropriate. While the virtues of experimental solution of static, elastic, two-dimensional problems are now largely overshadowed by analytical methods, problems involving three-dimensional geometry, multiple-component assemblies, dynamic loading and inelastic material behavior are usually more amenable to experimental analysis.

The name photoelasticity reflects the nature of this experimental method: *photo* implies the use of light rays and optical techniques, while *elasticity* depicts the study of stresses and deformations in elastic bodies. Through the photoelastic-coating technique, its domain has extended to inelastic bodies, too.

Photoelastic analysis is widely used for problems in which stress or strain information is required for extended regions of the structure. It provides quantitative evidence of highly stressed areas and peak stresses at surface and interior points of the structure — and often equally important, it discerns areas of low stress level where structural material is utilized inefficiently.

This chapter is intended to introduce the basic concepts — to emphasize those elements that are fundamental to the photoelastic method. The details involving characteristics of specific photoelastic materials — their formulation, optical and mechanical properties, machining techniques, etc. — and the details involved in the use of specialized auxiliary instruments and accessories are not included. While such information is vitally important to the student of photoelasticity, it quickly becomes obsolete and is better disseminated by current technical papers and current manufacturers' literature.

6.2. PHOTOELASTIC BEHAVIOR

The photoelastic method is based upon a unique property of some transparent materials, in particular, certain plastics. Consider a model of some structural part made from a photoelastic material. When the model is stressed and a ray of light enters along one of the directions of principal stress, a remarkable thing happens. The light is divided into two component waves, each with its plane of vibration (plane of polarization) parallel to one of the remaining two principal planes (planes on which shear stress is zero). Furthermore, the light travels along these two paths with different velocities, which depend upon the magnitudes of the remaining two principal stresses in the material.

Figure 6.1 illustrates this phenomenon. The incident light is resolved into components having planes of vibration parallel to the directions of the principal stresses σ_1 and σ_2. Since these waves traverse the body with different velocities, the waves emerge with a new phase relationship, or relative retardation.[2] Specifically, the relative retardation is the difference between the number of wave cycles experienced by the two rays traveling inside the body.

---

[1]Professor of Engineering Science and Mechanics, Virginia Polytechnic Institute and State University, Blacksburg VA 24061.

[2]The frequency of a monochromatic light wave is constant, regardless of the material being traversed by the wave. Therefore, the two waves have different wavelengths inside the body.

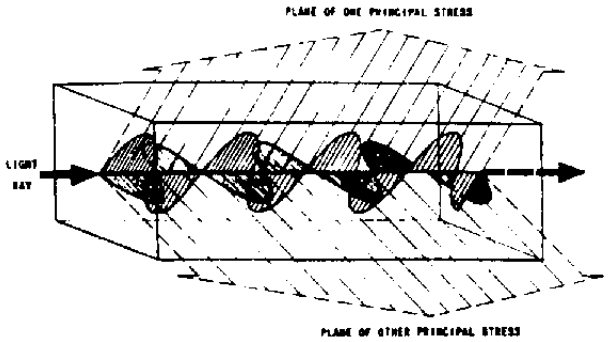

Fig. 6.1. Plane-polarized light waves double refracting model. 3 $\frac{3}{4}$ waves are shown for one plane, 3 $\frac{1}{2}$ waves for the other; relative retardation is $\frac{1}{4}$ wave.

This phenomenon is called double refraction or birefringence, and is the same as exhibited by certain optical crystals — but in photoelasticity the double refraction is artificial, being controlled by the state of stress or strain at each point in the body.

The two waves are brought together in the photoelastic polariscope, and permitted to come into optical interference. If the relative retardation $\overline{N}$ is 0, 1, 2, 3,... cycles, the waves reinforce each other, and the combined effect is a large light intensity.[3] If the phase difference $\overline{N}$ is $1/2, 3/2, 5/2, 7/2,...$ cycles, the amplitude of the two interfering waves is everywhere equal and opposite; destructive interference ensues, and the light intensity diminishes to zero (extinction). Intermediate intensities are developed for intermediate values of $\overline{N}$. Thus, a photoelastic pattern of dark and light bands, such as shown in Fig. 6.2, is formed as follows: the locus of points at which $\overline{N} = 0$ forms a light band: the locus of points at which $\overline{N} = 1/2$ forms an adjacent dark band; another light band is formed by rays traversing the photoelastic material at points where $\overline{N} = 1$; and successive dark and light bands are formed for increasing values of $\overline{N}$. In the nomenclature of optical interference, these bands are called *fringes*, and the *fringe order* is defined as the value of N along the band under consideration.

Fig. 6.2. Photoelastic pattern for wrench model.

6.3. TWO-DIMENSIONAL PHOTOELASTICITY

The foregoing is a rather general description of the formation of photoelastic patterns. It applies equally well to two-dimensional and three-dimensional photoelasticity and to the method of photoelastic coatings. Now, let us restrict the discussion to plane-stress systems, so that the basis of photoelasticity can be developed without needless complications. A plane-stress problem is approached when the thickness (lateral dimension) of the prototype and the model is small in relation to dimensions in the plane, and the applied forces act in the plane at midthickness (Fig. 6.3). For such a system, we are concerned with stresses acting parallel to the plane of the model only, for all other stress components are zero.

[3]This applies to a light-field circular polariscope with monochromatic light.

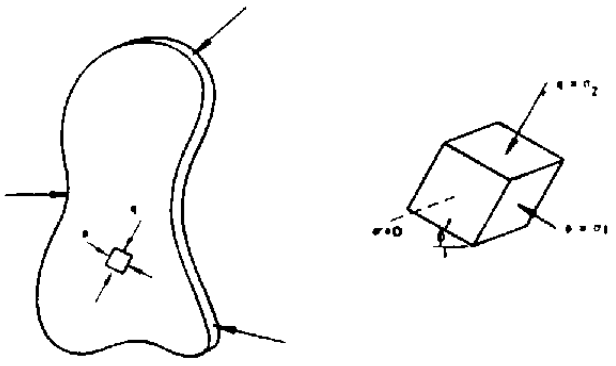

Fig. 6.3. Plane-stress system.

Mentally remove any small element, oriented such that the faces of the element are principal planes. The surfaces of the model are automatically principal planes (for no shear stress acts on these surfaces). Define the orientation of principal planes by the angle ϕ, and let σ_1 always represent the algebraically larger of the two principal stresses, such that $(\sigma_1 - \sigma_2)$ is always positive. The objective now is to show how stresses and stress directions are derived from photoelastic patterns.

6.4. THE ISOCHROMATIC PATTERN

Let us view a plane-stress model in a circular polariscope. A pattern of dark and light bands (Fig. 6.4) forms in the viewing screen when external forces or loads are applied to the model, and the number of these bands increases in proportion to the external forces. These patterns, which provide the value of N throughout the model, are appropriately called *isochromatic patterns*.

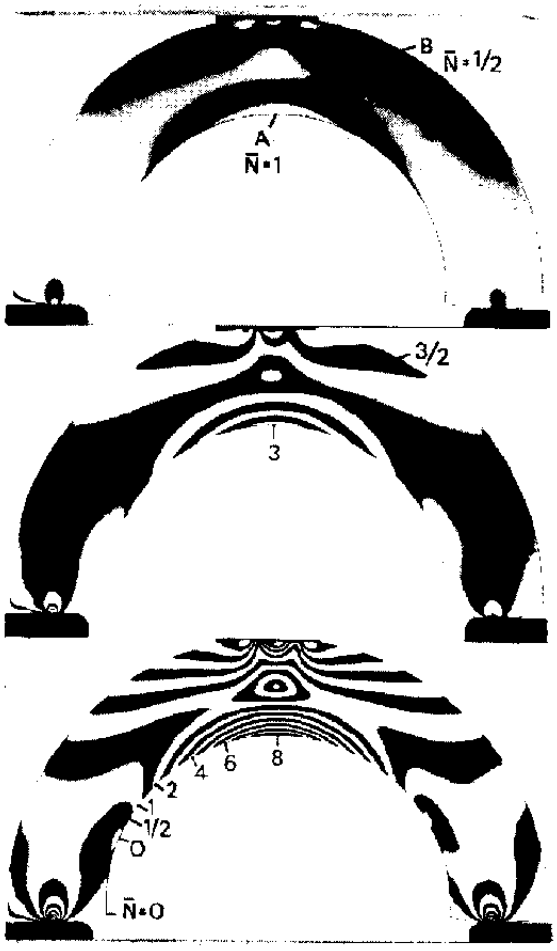

Fig. 6.4. For formation of the isochromatic pattern with increasing loads; centrally loaded arch.

The isochromatic pattern is related to the stress system by the stress-optic law. namely

$$\sigma_1 - \sigma_2 = \frac{f}{t}\overline{N} \tag{6.1}$$

where f is the stress-optical coefficient, a constant that depends upon the model material and the wavelength of light employed[4], t is the model thickness, and $\overline{N}$ is the relative retardation of rays forming the pattern. The term $\overline{N}$ is also known as *isochromatic fringe order*.

Equation (6.1) states that the relative retardation, $\overline{N}$, at each point in the model is directly proportional to the difference of principal stresses $\sigma_1 - \sigma_2$ at the point.

6.5. INTERPRETATION OF ISOCHROMATIC PATTERNS

Since $\sigma_1 - \sigma_2$ varies throughout the model in a continuous manner, $\overline{N}$ varies in a continuous manner. A change from a dark fringe to an adjacent light fringe represents an increase or decrease of 1/2 in the value of $\overline{N}$; to assign any other magnitude would violate the principle of continuity.

In terms of the isochromatic pattern, the isochromatic fringe order, $\overline{N}$, at a point is defined specifically as the number of fringes that pass through the point during the application of the external loads. Thus, at point A in Fig. 6.4, $\overline{N}$ increases with load from 0 to l, 3 and 8. Similarly, the number of fringes that passed through point B for these patterns is 1/2, 1 1/2 and 4. We can, therefore, observe the formation of the isochromatic pattern to determine $\overline{N}$ at any point. Alternately, we can learn to count fringes in an isochromatic pattern from a point of zero stress to any other point in the model. In this case, it is important to recognize whether the fringe order is increasing or decreasing along the path of the fringe count. Additional discussion appears under the heading "Free-boundary Stresses."

6.6. THE CIRCULAR POLARISCOPE

The formation of the photoelastic pattern has been described as a case of optical interference. Each ray that enters the model is divided into two components. and after emerging from the model they combine to yield either constructive or destructive interference. The relation between fringe order and light intensity is given by the equation of two-beam interference.[5]

$$I = a^2 \cos^2 \pi\overline{N} \tag{6.2}$$

However, it is well established and demonstrated in elementary courses on light that waves *cannot* combine to yield optical interference unless they are coherent and are polarized in the same plane. The *photoelastic polariscope* serves to bring these waves into a common plane, so that optical interference can ensue. The polariscope does not rotate the planes of polarization of these rays, but instead, it transmits only those components of the two interfering rays that lie in a common plane (plane of polarization of the analyzer). For example, let the arrows y_1 and y_2, in Fig. 6.5, represent the planes of polarization of the two wave components. If the rays are passed

---

[4]The constant f is a lumped constant, viz., $f = \lambda/(C_1 - C_2)$, where λ is the wavelength of monochromatic light used in the experiment and C_1, C_2 are independent constants of the photoelastic material — which can be derived from measurements of the two velocities of light propagation through the stressed material.

[5]Equation (6.2) applies for a light-field circular polariscope: for dark field, $I = a^2 \sin^2 \pi\overline{N}$ and the complementary pattern is formed.

through a polarizing medium (such as a Polaroid plane-polarizing sheet) oriented with its transmission axis horizontal, the vertical component of these waves will be stopped (absorbed) and the horizontal components, y_3, and y_4, transmitted. Now y_3, and y_4 are waves polarized in a common plane, and they can combine to produce optical interference.

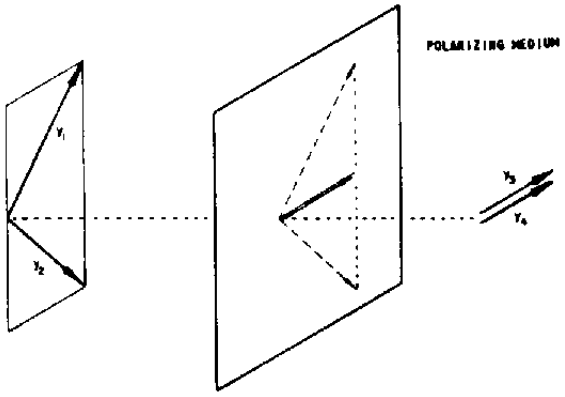

Fig. 6.5. Transmission of coplanar wave components by a polarizing agent.

The apparatus employed to exhibit isochromatic patterns is called a circular polariscope, shown schematically in Fig. 6.6. Several other versions of the photoelastic polariscope have been advanced [1, p. 382], notably the *diffused-light* polariscope and the reflection or *doubling* polariscope. The lens-system polariscope, however, is generally accepted as the most versatile instrument for photoelastic investigations.

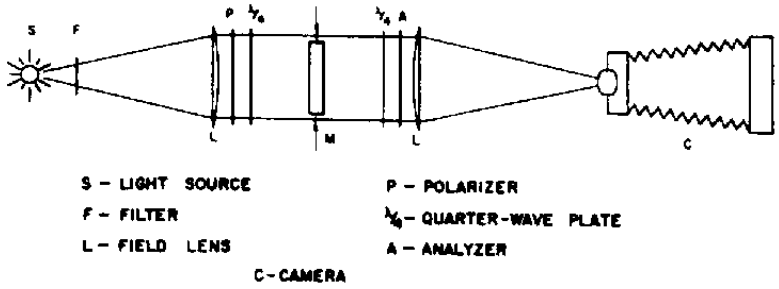

Fig. 6.6. Lens-type circular polariscope.

The polariscope components can be divided into two categories; elements that direct and focus the light rays, and elements that control the wavelength and polarization of the waves. The two field lenses and the camera lens are in the first category. The first field lens is located such that the light source lies at its focal point; thus, a parallel or *collimated* beam of light issues from the field lens into the model zone. The second field lens converges this beam so that all the light enters the camera lens. The camera, in turn, is focused to project an image of the model onto the camera screen or photographic film.

In the second category, a color filter is usually employed to isolate a small band of wavelengths by absorbing all colors except that which is desired. The functions of the polarizing elements, polarizer, quarter-wave plates and analyzer are shown in Fig. 6.7. The polarizer divides the incident light waves into vertical and horizontal components. It absorbs all the vertical components and transmits the remaining plane-polarized light (horizontal).

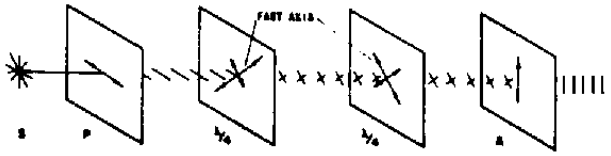

Fig. 6.7. Polarization of light waves in a circular polariscope

A quarter-wave plate is a member that behaves exactly like a photoelastic model having uniform birefringence of $\overline{N} = 1/4$.[6] It is oriented with its principal planes (or principal axes in this case) at an angle of 45° to the axis of the polarizer. The purpose of the quarter-wave plate is to supply equal quantities of light along each of the two planes of polarization at every point in the model. Ordinarily, the quarter-wave plates are crossed, i.e., the plane of polarization of the higher-velocity waves in the first plate coincides with the plane of the slower waves in the second quarter-wave plate.

The analyzer is actually a second polarizer. If it is oriented with its polarizing axis crossed to the axis of the polarizer, a *dark-field* isochromatic pattern is formed, as in the right-hand pattern of Fig. 6.8. Then, the centers of *dark* fringes are points of integral values of $\overline{N}$ ($\overline{N}$ = 0, 1, 2, 3,...). If the polarizer and analyzer axes are parallel, a *light-field* isochromatic pattern is formed, and the centers of light fringes are points of integral values of $\overline{N}$ (see Fig. 6.8, left). The light-field pattern is generally preferred, for then the model boundaries are clearly defined.

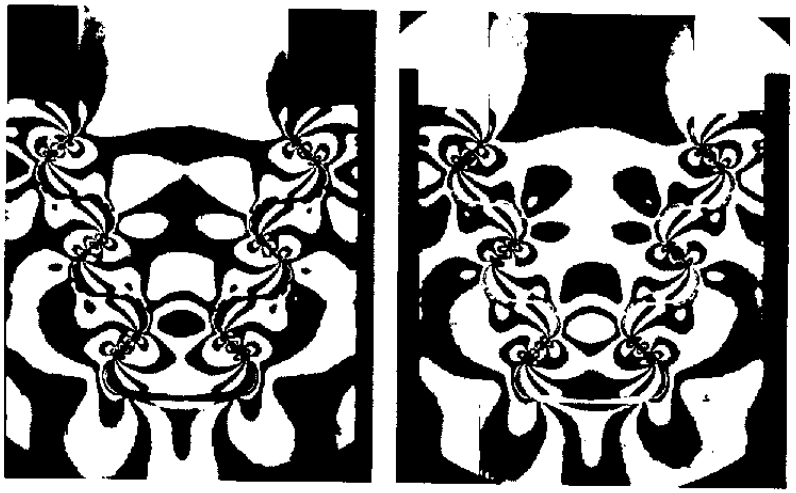

Fig. 6.8. Isochromatic patterns for two-dimensional analysis of dovetail joint. Left—dark field; right—light field.

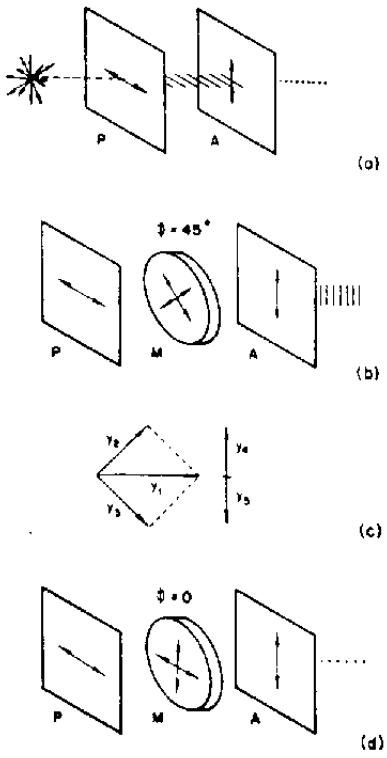

Fig. 6.9. Polarization of light waves in a plane polariscope.

[6]The discussion thus far implies the use of monochromatic light.

6.7. DIRECTIONS OF PRINCIPAL STRESS

If we remove the quarter-wave plates from the polariscope described above. we are left with the system shown schematically in Fig. 6.9. Plane-polarized light (horizontal) passes through the region between polarizer and analyzer. If the polarizing axis of the analyzer is horizontal. this light passes through the system; if the axis is vertical, however, the light is stopped by the analyzer and complete extinction results. Next, insert a model between the elements such that the direction of principal stresses is at an angle $\phi = 45°$ from the vertical. Upon entering the model, the plane-polarized light y_1, (see Fig. 6.9(c)) is divided into two components, $y_2 = y_1 \sin\phi = y_1 / \sqrt{2}$ and $y_3 = y_1 / \sqrt{2}$ and these components traverse the model. Components of y_2 and y_3 that lie in a vertical plane are capable of passing through the analyzer. Indeed, these components, y_4 and y_5, are transmitted by the analyzer, and they combine to form an optical interference pattern which depends upon the values of $\overline{N}$ introduced by the model. This is, of course, the now familiar isochromatic pattern.

In the last diagram of Fig. 6.9, the arrangement is similar, except here the model is oriented such that the principal-stress directions are parallel to the axes of the polarizer and analyzer ($\phi = 0°$). The model resolves the incident light into components parallel to the principal-stress directions, but in this case there is no component of the incident light in the vertical direction. All the light is transmitted with a horizontal plane of vibration. Upon reaching the analyzer, there is still no component in the vertical direction, and the light is completely extinguished. Thus, for the condition $\phi = 0°$, all light is extinguished regardless of the value of $\overline{N}$.

6.8. ISOCLINICS

In general, the directions of principal stresses vary continuously from point to point in a photoelastic model. Conditions depicted in Figs. 6.9(b) and (d), therefore, occur simultaneously at different regions in the model. Again, since changes in stresses and stress directions occur in a continuous manner in a body, points at which the principal stresses have a common direction lie along a continuous curve. For any orientation of the model, the focus of points at which $\phi = 0°$ forms a continuous black (extinction) curve, called an *isoclinic*, or an *isoclinic fringe*. Elsewhere, for values of ϕ not equal to zero, the isochromatic pattern is present.

Isoclinics are developed in a plane polariscope, which is merely a circular polariscope with the quarter-wave plates removed; the axes of polarization for polarizer and analyzer are crossed. The equation of intensity distribution in the case of a plane polariscope is

$$I = a^2 \sin^2 2\phi \sin^2 \pi\overline{N} \tag{6.3}$$

It is immediately evident that the emergent intensity is zero at every point where 0 is zero, regardless of the value of $\overline{N}$. In addition, $I = 0$ when $\overline{N} = 0, 1, 2, 3,...$ and this prescribes the formation of isochromatic fringes in regions of $\phi \neq 0°$. In essence, the plane polariscope yields the isochromatic pattern, but the intensity of this pattern is modulated by the isoclinic term $\sin^2 2\phi$.

A photoelastic pattern produced in a plane polariscope is shown in Fig. 6.10(a). This shows the zero-degree isoclinic, together with the isochromatic pattern. Obviously, the pattern is ambiguous, for one cannot distinguish the isoclinic curve from the isochromatics. This problem can be minimized by employing white-light illumination. In white light, the isochromatic pattern is everywhere colored, except at points for which $\overline{N} = 0$. For $\phi = 0°$, however, extinction prevails for all wavelengths, and the isoclinic is always black. Figure 6.10(b) shows the same zero-degree isoclinic, photographed with white-light illumination on panchromatic film.

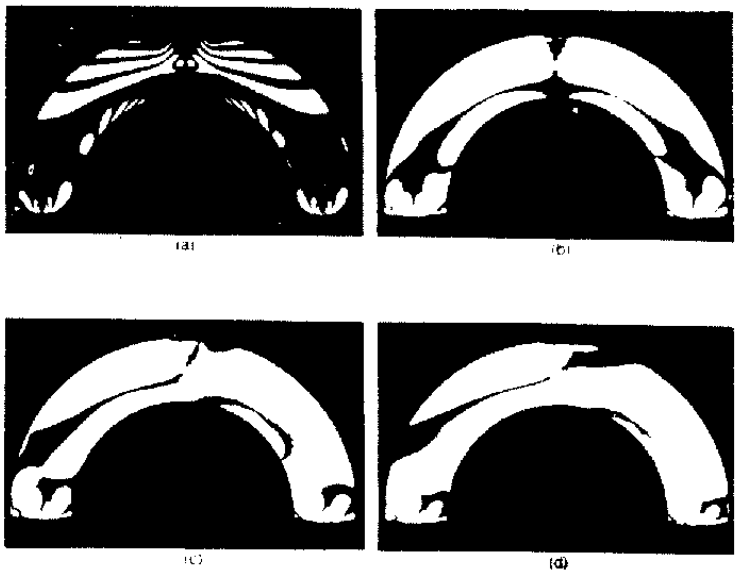

Fig. 6.10. Isoclinic fringes in centrally loaded arch model: (a) and (b)—0 deg; (c)—10 deg; (d)—20 deg.

If the polarizer and analyzer are maintained in the crossed position and rotated together through 90° while the loading remains constant, an isoclinic fringe will pass through every point in the model. This is evident since, sometime during the rotation, the polarizer and analyzer axes must be parallel to the principal-stress directions at each and every point in the model. In order to determine the principal-stress directions throughout the model, the isoclinic fringes are recorded for successive angular positions of the polarizer and analyzer. Photographs of isoclinics taken with the polarizer and analyzer rotated through 10° and 20° are shown in Figs. 6.10(c) and (d).

6.9. WHITE-LIGHT ILLUMINATION

Equations (6.1) and (6.2) imply the use of monochromatic light in an experiment. We can investigate the effect of white-light illumination, that is, simultaneous illumination by all the wavelengths of the visible spectrum, by using these equations and the footnote to eq (6.1). Thus, for each wavelength, it can be shown that,

$$\overline{N} = \frac{(\sigma_1 - \sigma_2)t(C_1 - C_2)}{\lambda}$$

and substituting into eq (6.2)

$$I = a^2 \cos^2\left[\pi(\sigma_1 - \sigma_2)(C_1 - C_2)\frac{t}{\lambda}\right]$$

Since $t(C_1 - C_2)$ is a constant in any given experiment,[7] from point to point as a function of wavelength λ (or the color of the light) and stress parameter $\sigma_1 - \sigma_2$. Waves of different wavelength do not interact. Instead, each wavelength displays its own intensity pattern in its own color. The result is superposition of patterns for all the wavelengths employed. At any point in the model, the shade (or combination of colors) is a unique function of $\sigma_1 - \sigma_2$ and adjoining points of equal $\sigma_1 - \sigma_2$ comprise a band in the colorful isochromatic pattern.

[7]This is a first approximation. Actually C_1-C_2 does vary with wavelength λ; this effect is called dispersion of photoelastic constants with wavelength.

Aside from their aesthetic beauty, white-light isochromatic patterns permit accurate determination of $\sigma_1 - \sigma_2$. This is useful if isochromatic fringe orders are low, e.g., $\overline{N}$ = 3 or less, whereas it is unnecessary if the maximum isochromatic fringe order is high. The human eye can discern variations in color with greater sensitivity than it can detect the maximum- or minimum-intensity points in a monochromatic pattern. In practice, color matching is employed, using a separate calibration sample in which color is known as a function of $\overline{N}$. Sensitivity is further augmented if observations are restricted to the positions of the purple bands — termed 'tints of passage' for the first three fringe orders. These occur as very narrow, sharply defined purple bands between red and blue fringes in the isochromatic pattern, and the positions of the tint-of-passage fringes can be ascertained with high precision.

6.10. DETERMINATION OF FRACTIONAL FRINGE ORDERS

For isochromatic patterns from monochromatic light, the distribution of fringe order ($\overline{N}$) along any line can be plotted by ascertaining the positions of the centers of integral and half-order isochromatic fringes that cross the line. High accuracy is obtained directly from fringe photographs in cases where a large number of fringes cross the region of interest. For cases in which the maximum fringe order is low, or the variation of fringe order is low, we cannot be content with integral and half-order fringe locations. Instead, the ability to locate points of intermediate or partial values of $\overline{N}$ (fractional or decimal values) is required.

In general, the method of partial-fringe measurement can be broken into three categories, namely, compensation, analyzer rotation and fringe multiplication. They are characterized by a common objective — the modification of eq (6.2), such that intensity maxima and minima occur not merely at integral and half-order values of relative retardation in the model, but also at intermediate points. Analyzer rotation and compensation are point-by-point methods, since the direction of principal stresses must be determined at each point before its fractional fringe order is measured. Fringe multiplication is a full-field method. All three methods enhance the sensitivity of data retrieved by about one order of magnitude.

6.10.1. Analyzer Rotation

The method of analyzer rotation has the advantage that no additional equipment is required. A dark-field circular polariscope using monochromatic light is employed. First the quarter-wave plates arc removed and the polarizer and analyzer are rotated together until an isoclinic fringe is centered on the point being measured in the stressed photoelastic model, e.g., point *A* in Fig. 6.11. Thus, the polarizer and analyzer are aligned with the principal stress directions at *A*. Next, the quarter-wave plates are reinserted with their usual 45° alignment for dark-field circular polarization and fringes such as those in Fig. 6.11(a) are observed. Then, by rotating the analyzer (only the analyzer) while viewing the fringes, we find that either of the neighboring fringes can be moved to point *A*, as indicated in Fig. 6. 11.

The relationship governing the distribution of light intensity may be derived—with the result

$$I = a^2 \sin^2\left(\pi\overline{N} + \beta\right) \tag{6.4}$$

where β is the angle of analyzer rotation from the normal (crossed) position. Thus, by rotating the analyzer, we observe an extinction of light (I = 0) when

$$\left(\beta + \pi\overline{N}\right) = 0°, 180°, 360°, \text{etc.}$$

For example, consider Fig. 6.11. At point A, let $\overline{N} = 2\frac{1}{3}$ fringes; therefore $\pi\,\overline{N} = (180°)\left(2\frac{1}{3}\right)$=420°. Extinction occurs when $\left(\beta + \pi\overline{N}\right)$ = 360° or 540°. For the case of 360°, β = 360°-420° = -60° and β/π corresponds to 60°/180° or 1/3 of a fringe order. Similarly, for the case of 540°, β = 540°-420° = 120°, as indicated in the figure. Then $\beta/\pi = \frac{2}{3}$ fringe. Thus, the fringe order is established as 1/3 fringe from second order or $\frac{2}{3}$ fringe from the third order, namely $2\frac{1}{3}$ fringes.

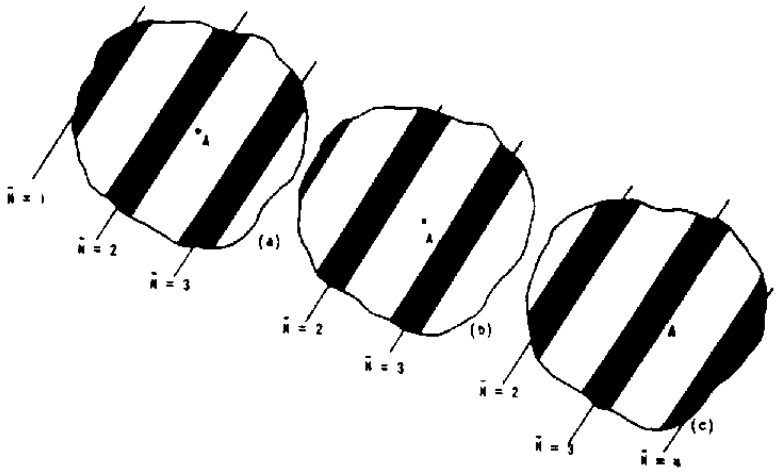

Fig. 6.11 Fractional fringe orders by analyzer rotation: (a) before analyzer rotation; (b) motion of fringes during analyzer rotation; (c) after analyzer rotation.

To formalize the argument, let β be positive for analyzer rotation that brings the higher-integral-order neighboring fringe, or order M, to the point under consideration. Then, $I = 0$ when

$$\beta + \pi\overline{N} = \pi\overline{M}$$

and, therefore,

$$\overline{N} = \overline{M} - \beta/\pi$$

Photometric devices can be used if desired to ascertain the intensity minima, i.e., when the center of a fringe is at the point in question. Measurements to 1/100th of a fringe order can be made with photocell apparatus, while a similar accuracy is possible by visual observation only if great care is taken.

The method of analyzer rotation described here is also known by other names, notably, the *Tardy Method*.

6. 10.2. Compensation

In compensation, we add to the birefringence of the model, at some given point, an equal and opposite birefringence such as to bring the total relative retardation to zero. This is done by placing an instrument — a compensator — in the optical path adjacent to the model, as shown in Fig. 6.12. The compensator is adjusted to bring the center of a zero-order fringe to some given point on the photoelastic model and the fringe order contributed by the compensator is read off the instrument. Of course, this corresponds to the fringe order in the model, too.

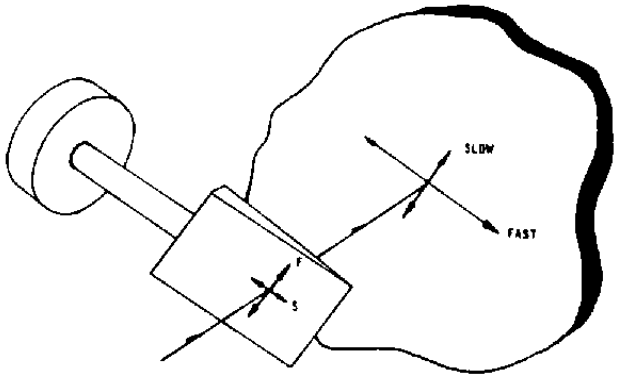

Fig. 6.12. Nullification of relative retardation by compensation.

The active element of the compensator is usually a wedge of a permanently birefringent crystal which is moved across any given point in the model until compensation, or zero relative retardation is achieved: alternatively, a photoelastic model with a simple predetermined stress system is used as the active element. The simple wedge, the Babinet compensator and the Babinet-Soleil compensator are in this category. Equivalent instruments have been made in photoelastic laboratories using a strained photoelastic specimen in place of the crystal [1, pp. 163-166].

6.10.3 Fringe Multiplication

Fringe multiplication is achieved by passing the light back and forth through the model, so that the relative retardation occurring in each passage is accumulated and the sum is displayed in the multiplied isochromatic pattern. Figure 6.13 shows an example in which the basic specimen exhibits very low relative retardation. The patterns labeled 1×, 5× and 11× are. respectively, the ordinary isochromatic pattern, the five-times multiplied pattern from light passing five times through the same specimen, and the eleven-times multiplied pattern for the same specimen. The inserts show enlarged views of the stress concentration zone for the 5× and 11× patterns, revealing that the method does not sacrifice fringe resolution.

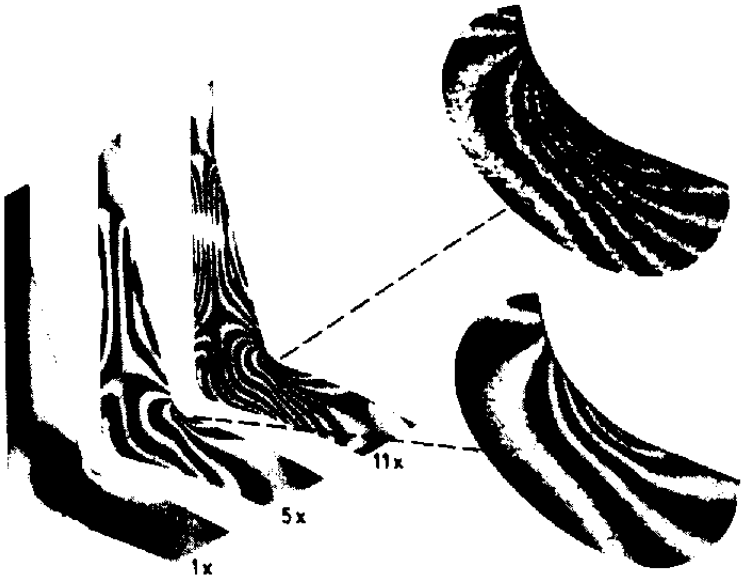

Fig. 6.13. Isochromatic patterns illustrating photoelastic fringe multiplication by factors of 1, 5 and 11. Specimen is a thin slice from a frozen-stress model of a spherical pressure vessel with a cylindrical nozzle and shows the stress distribution and stress concentration at the junction between the vessel and nozzle.

Fringe multiplication is accomplished by installing a partial mirror on each side of the model-mirrors that reflect about 85 percent of the incident light and transmit about 15 percent — as shown in Fig. 6.14. The mirrors are slightly inclined, so that the light beams emerge in slightly

different directions according to their number of passages through the model. Light passing through the model 1, 3 and 5 times is converged to points a, b and c, respectively. A plate with a small hole stops all the unwanted beams and allows only the beam carrying the desired multiplication pattern to pass into the eye of the observer (as shown) or into a camera. In the figure, the 7× pattern would be viewed.

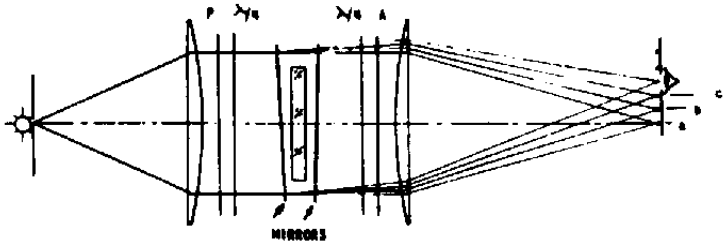

Fig. 6.14. Optical system for fringe multiplication.

With fringe multiplication, the stress-optic law becomes

$$\sigma_1 - \sigma_2 = \frac{f}{t}\frac{\overline{N}}{\alpha} \tag{6.5}$$

where α is the fringe-multiplication factor, or the number of times light passed through the model, and $\overline{N}$ is the fringe order read off the multiplied pattern.

Fringe multiplication is applicable to both two-dimensional models and slices taken from frozen-stress three-dimensional models. However, the need for enhancement of sensitivity of measurements is less frequently required in two-dimensional work. Figure 6.13 is an example taken from a three-dimensional problem [2,3].

6.11. INTERPRETATION OF PHOTOELASTIC DATA

6.11.1. Calibration

The principal-stress difference $(\sigma_1 - \sigma_2)$ at each point in the model is proportional to the birefringence $\overline{N}$ at the point. But what is the constant of proportionality? This can be determined by an experiment in which all quantities are known (or measured) except that constant. Thus, a very simple model, for example, a bar in pure tension or a beam in pure flexure, may be chosen. In these cases the principal stresses are well known in terms of the dimensions of the model and applied load. The model thickness and fringe order are measured, and the stress-optical coefficient is computed by eq (6.1) as

$$f = t(\sigma_1 - \sigma_2)\frac{1}{\overline{N}}$$

Normally, calibration bars are cut from the same sheet or batch of photoelastic material as the corresponding photoelastic model, and the calibration measurement is performed with the same light source as the model measurements, for f is a function of both the model material and the wavelength of the light used.

6.11.2. Free-boundary Stresses

The magnitude of $\sigma_1 - \sigma_2$ is derived throughout the member from the isochromatic pattern. However, at free boundaries, that is, boundaries along which no external forces are

applied, one of the principal stresses is zero. Therefore, the remaining principal stress is determined uniquely by the isochromatic fringe order. As shown in Fig. 6.15, the designation of boundary stresses must be consistent with the proposition that $\sigma_1 > \sigma_2$. Free-boundary stresses play a very important role in stress analysis, for the critical stress in a body very frequently occurs at a boundary point.

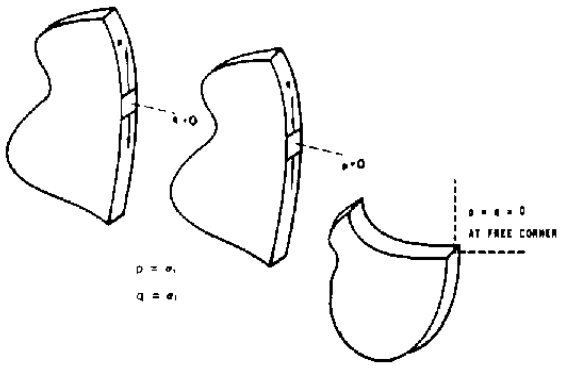

Fig. 6.15. Free-boundary stresses.

At a free external corner, the complete absence of external forces must be accompanied by the complete absence of internal resistive forces, or stresses. Thus $\sigma_1 = \sigma_2 = 0$ at external comers and the isochromatic fringe order is always zero; this holds equally true for dynamic and three-dimensional stress systems, as well as for static two-dimensional stress systems. An example of $\overline{N} = 0$ at a free comer appears in Fig. 6.4. Advance knowledge of a fringe order at some point is often extremely helpful in interpreting an isochromatic pattern from a photograph, particularly when the development of the pattern during load application is not observed.

Free boundaries provide additional clues for ascertaining fringe order from photographs of isochromatic patterns. The engineer can usually surmise from the model geometry and loading whether boundary stresses are tensile or compressive, and whether stress along a boundary is increasing or decreasing. This together with knowledge of fringe orders at one or more points and knowledge that fringe orders change In a continuous, orderly fashion, usually allows the experimenter to establish stress values along boundaries. Since the fringe order is constant along any isochromatic band, determination of fringe orders at all points within the model is then a simple step; instances in which an isochromatic band intercepts model boundaries at more than one point provide valuable check points.

6.11.3. Stress Trajectories

Maps showing the directions of principal stresses in loaded members are valuable aids for understanding stress systems. By studying such stress-flow diagrams, or *stress-trajectory* diagrams, an engineer can develop a talent for predicting the stress system in a part prior to formal analysis.

Stress trajectories are paths comprised of points et which the principal-stress directions are tangent to the path. An orthogonal network is formed by the two families of trajectories one everywhere tangent to σ_1, and the other to σ_2.

A set of isoclinic, e.g. zero to 80° isoclinics in 10° increments, provides the data to draw stress trajectories. Manual graphical techniques are available [1, pp. 198-214], an optical photographic technique has been devised [4], and graphing by computer is feasible.

6.11.4. Complete Stress Solution at Interior Points

For some problems it is important to determine the complete state of stress at interior points. The complete state of stress is determined by three quantities: σ_1, σ_2 and ϕ. However, the

photoelastic methods discussed above provide only two quantities, namely $(\sigma_1 - \sigma_2)$ and ϕ. Thus, the isochromatic pattern and the isoclinic curves are not sufficient, by themselves, to provide the complete stress solution for interior points. Supplementary information must be provided, and this additional information may take various forms.

Numerous methods have been developed to provide the third quantity. The oblique-incident method [5] employs a second or additional measurement of fringe order, but with the light ray traversing the model along an oblique line with respect to the model surface. Thus, a supplementary relationship between stresses and measured fringe order is obtained. which together with knowledge of $\sigma_1 - \sigma_2$ and ϕ, permits calculation of the individual principal stresses σ_1 and σ_2. In theory, any direction of oblique incidence can be used but, for practical reasons, the plane of incidence (the plane containing the incident oblique ray and the normal to the plane of the model) is usually oriented to contain one of the principal-stress directions.

Other methods employed to provide the third required piece of information make use of relationships derived in the theory of elasticity which must be satisfied by every elastic system. The shear-difference and the numerical-iteration methods fall into this category. While these involve tedious calculations, particularly if data are processed for a closely spaced network of lines, they have been used in the solution of many important problems. Today, labor can be reduced by use of modern computers to perform these readily programmed computations.

Still other methods developed to provide the supplementary information for the complete stress solution include several electrical and mechanical analogs of the stress system.

Isopachic methods provide the third piece of information by measurements of change of thickness of the model. For two-dimensional states of stress, lateral strain or change of thickness is proportional to $\sigma_1 + \sigma_2$. This, together with photoelastic measurements of $\sigma_1 - \sigma_2$, permits calculation of individual values σ_1 and σ_2. Various mechanical, electromechanical and optomechanical extensometers have been developed for point-by-point measurements of these changes of thickness. Full-field optical-interference methods can also be used to measure change of thickness [6], but here a second model is required using material whose refractive index does not change with stress, e.g., methylmethacrylate (Plexiglas, Lucite, etc.). The locus of points along a model having constant lateral strain or constant $\sigma_1 + \sigma_2$ is called an *isopachic* contour.

If a photoelastic model is used in an interferometer, the interference fringes are a function of the changes of velocity of light as well as the changes of model thickness. Since there are two velocities of light (with different planes of polarization) for each point in the model, two superimposed fringe patterns emerge from the interferometer. These yield sufficient information to calculate the individual principal stresses σ_1 and σ_2. All interferometric measurements utilizing photoelastic models are in the category called *absolute-retardation measurements*, as distinguished from relative-retardation measurements. The absolute-retardation methods are especially valuable for dynamic studies, since complete information to calculate σ_1 and σ_2 throughout the field is obtained in one photograph. Numerous optical interferometers, especially the Series Interferometer, and the more recently developed method of holographic interferometry, may be used for absolute-retardation measurements [7].

6.11.5. Transition from Model to Prototype

The photoelastic method yields stresses in the model itself. How are these related to stresses in the prototype? For many practical two-dimensional elastic problems with forces applied to external boundaries, stresses depend upon geometry and external forces only, and not upon the physical properties of the material (except, of course, that the material must be elastic, homogeneous and isotropic).

A model must then be geometrically similar to the prototype, but not necessarily of the same size; the loads must be similarly distributed, but they may differ in magnitude by a factor of

proportionality. Any stress, σ, in the prototype is determined from the corresponding stress, σ_m, at the corresponding point in the model by

$$\sigma = \frac{FL_m^2}{F_m L^2}\sigma_m \tag{6.6}$$

where F is a force applied to the prototype, L is a linear dimension in the prototype, m = a subscript denoting corresponding values for the model.

Distorted models are often used for two-dimensional analyses, i.e. models that are geometrically similar to the prototype except for the plate thickness; any convenient model thickness can be used. In this case, the model law is

$$\sigma = \frac{FL_m t_m}{F_m L t}\sigma_m \tag{6.7}$$

where t_m and t represent model and prototype thickness, respectively.

Special consideration must be given to the question of Poisson's ratio match. Except for the case of all simply connected bodies and certain types of multiple-connected bodies in plane stress without body forces, true similitude requires equal Poisson's ratios for model and prototype materials. Fortunately, most photoelastic materials exhibit Poisson's ratio values between 0.3 and 0.35, which is close to that of structural metals; the small differences appear to be inconsequential. However, for materials that are suitable for the frozen-stress method (to be discussed later), which is used primarily in three-dimensional photoelastic studies, the effective value of Poisson's ratio is nearly 0.5. Several investigations have shown that this mismatch is responsible for dissimilarities in stresses between model and prototype, these differences amounting to a few percent of the peak-stress values. Accordingly, the photoelastic models exhibited erroneous stress distributions in regions of low stresses, but the determinations of high stresses were substantially correct.

6.12. TWO-DIMENSIONAL MODELS

Hard plastics for photoelastic models are characterized by a modulus of elasticity from about 300,000 to 500,000 psi (2.1 GPa to 3.5 GPa). They are generally brittle, exhibiting linear stress-strain behavior as well as linear strain-birefringence behavior to stress levels approaching the ultimate strength. Polyester resins such as Paraplex and Homalite 100, allyl resins such as CR-39, and various epoxy formulations are in this category. Epoxy resins are often favored because of their high photoelastic sensitivity and increased freedom from mechanical and optical creep. The others are colorless resins that offer glass-like surfaces similar to the plate-glass molds in which they are cast.

Soft plastics, characterized by moduli of elasticity of the order of 5000 psi (0.345 MPa), have found primary application in dynamic photoelasticity. Elastic wave propagation is much smaller in these low-modulus materials, permitting use of relatively common high-speed cameras in the 10,000-frames/s class. Urethane rubbers are most common, while highly plasticized epoxy formulations have also been used. Both exhibit viscoelastic behavior, rather than unique mechanical and optical constants.

Models having clear surfaces can be used without surface treatment, while those with diffusing surfaces require special attention. Surfaces can be ground and polished with fine abrasives and rouges. Alternately, they can be coated with oil or light grease to fill the minute irregularities and thus exhibit optically smooth surfaces. Epoxy and urethane plates that are cut from thicker slabs require such treatment. When these resins are cast against smooth Teflon

molds or molds having smooth layers of mold-release agents, the model surfaces are usually adequately clear for direct use.

Machining these model materials is best accomplished with carbide burrs or milling cutters driven at 5000 to 50,000 rpm. A quick and easy model-making procedure consists of first cutting the model 1/16 to 1/8 in. (1.5 to 3 mm) oversize with a bandsaw or jigsaw. The part is then attached to a metal template with double-faced pressure-sensitive tape. The model and template composite is placed on a high-speed routing machine in which a plug is fixed to the table directly below the cutting tool. The model is manually advanced into the cutter in a series of tangential strokes until the template contacts the plug. The plug then acts as a limit stop, and the model matches the template when the plug touches the template everywhere along its periphery. Both hard and soft plastics are machined by this method.

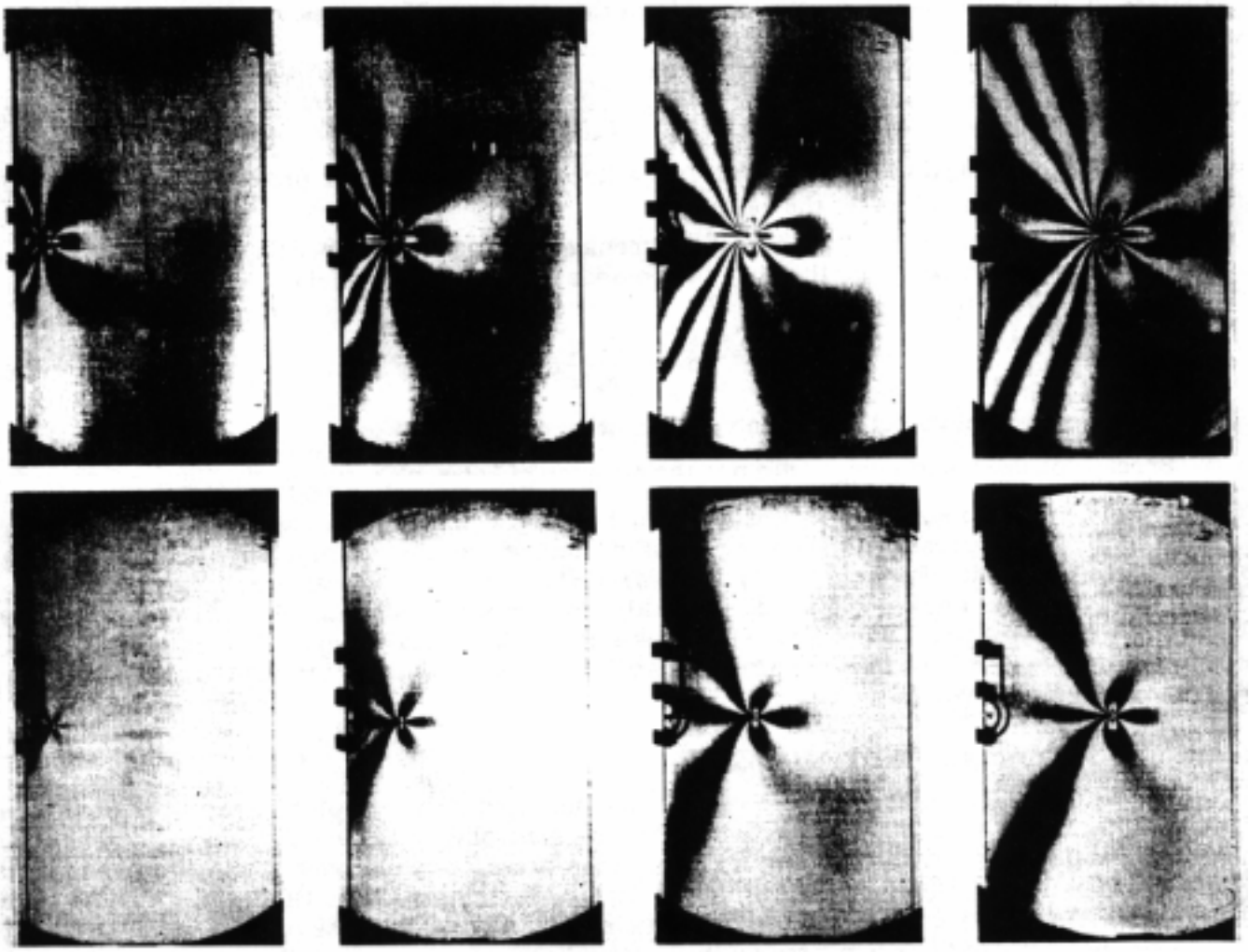

Fig. 6.16. Sequence of isochromatic patterns during dynamic crack propagation. Exposure 1 μs. Top row: 3× fringe multiplication.

Machining stress and associated birefringence are induced along model boundaries if excessive pressure and excessive heating are permitted. Sharp tools, high speeds and moderate feeds give stress-free models.

All model materials absorb moisture from the atmosphere. Moisture absorbed at newly cut edges causes swelling or volumetric expansion of material along the boundaries, inducing local compressive stresses and accompanying birefringence. Similarly, moisture lost along newly cut boundaries causes tensile boundary stresses. This buildup of extraneous birefringence is a time-dependent effect, the so-called 'time-edge effect'. It can be eliminated by keeping the material at

fixed humidity before and after machining, so that the moisture content in the material remains at equilibrium with the atmosphere. The time-edge effect can be minimized by immediately coating the model edges with a waterproofing agent, such as a silicone coating. Most generally, however, the time-edge effect is circumvented by performing the test within a few hours after the model is machined, thus precluding the buildup of substantial boundary birefringence.

6.13. DYNAMIC PHOTOELASTICITY

The techniques of two-dimensional photoelasticity apply to dynamic as well as static loading conditions [8,9]. The maximum permissible exposure time is determined by the time rate of change of fringe order and the fringe broadening (blurring) that can be tolerated. The first factor depends upon model geometry, thickness and sensitivity, velocity of elastic-wave propagation, and on loading rate and load magnitude. Fringe broadening of about one-fourth the separation between adjacent fringes is usually acceptable.

Hard plastics are usually employed, wherein the velocity of elastic waves is about 5000 fps. With these, exposure time of 1 μs is usually tolerable, although exposure as short as 0.1 μs are sometimes required. Soft plastics allow exposures 10 to 40 times longer.

Several different types of recording systems are applicable: optomechanical framing cameras of many different designs and capabilities, single-flash photography, the Cranz-Schardin multiple-flash system, the streak-camera technique, and the photometer technique. The first three yield full-field photoelastic patterns and, consequently, require large quantities of light. In the last two methods, variations of relative retardation with time are recorded for a single line and a single point in the specimen, respectively.

The sequence of dynamic events shown in Fig. 6.16 utilized the Cranz-Schardin system. They reveal the isochromatic patterns in a plate under tensile forces during catastrophic crack propagation 1101. The crack tip was advancing at nearly 2000 ft/s (610 m/s), approaching a theoretical crack-velocity limit. Elastic-wave velocity was about 5000 ft/s (1500 m/s). The lower row shows ordinary isochromatic patterns for four stages of crack growth, and the upper row shows the identical events, but with light that passed through the model three times instead of once. This multiplication of sensitivity produced much more satisfactory field cover, allowing more meaningful assessment of the dynamic events.

The optical system is shown in the top view of Fig. 6.17. Light from each spark source was collimated in the model zone and then converged to enter one of several camera lenses. Light from each spark was directed into a different camera lens. High-voltage sparks were discharged at predetermined intervals and the patterns occurring at the corresponding instants were recorded on a stationary film. Thus a high-speed photographic system was achieved without use of any moving parts!

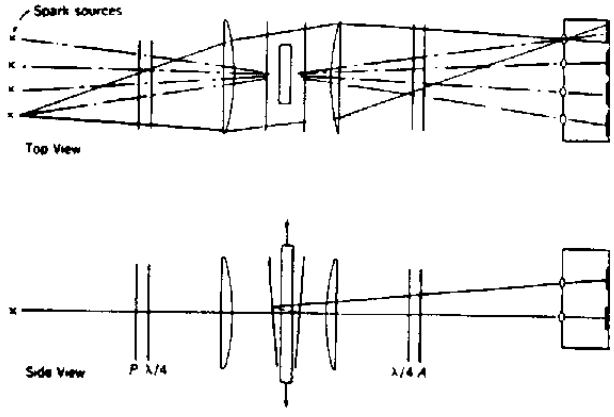

Fig. 6.17. Cranz-Schardin optical system for high-speed photography, modified for fringe multiplication.

The modification for fringe multiplication is shown in the side view. Two partial mirrors straddled the model, each slightly inclined so that light passing through the model three times was collected by a second row of four camera lenses. Thus, light from one spark discharge produced both the 1× and 3× patterns simultaneously.

Figure 6.18 shows an extremely interesting sequence of photoelastic patterns representing stresses in a semi-infinite plate subjected to a localized impulse load at the edge. Only a portion of the plate is visible, with the zone of load application at the upper right. Short-duration loading show how stress waves radiate out from the localized disturbance and travel through the plate with an orderly discipline. This is an excellent illustration of the separation of waves that travel with different velocities through elastic solids. A 16-frame Cranz-Schardin camera was used, although only four frames are shown here.

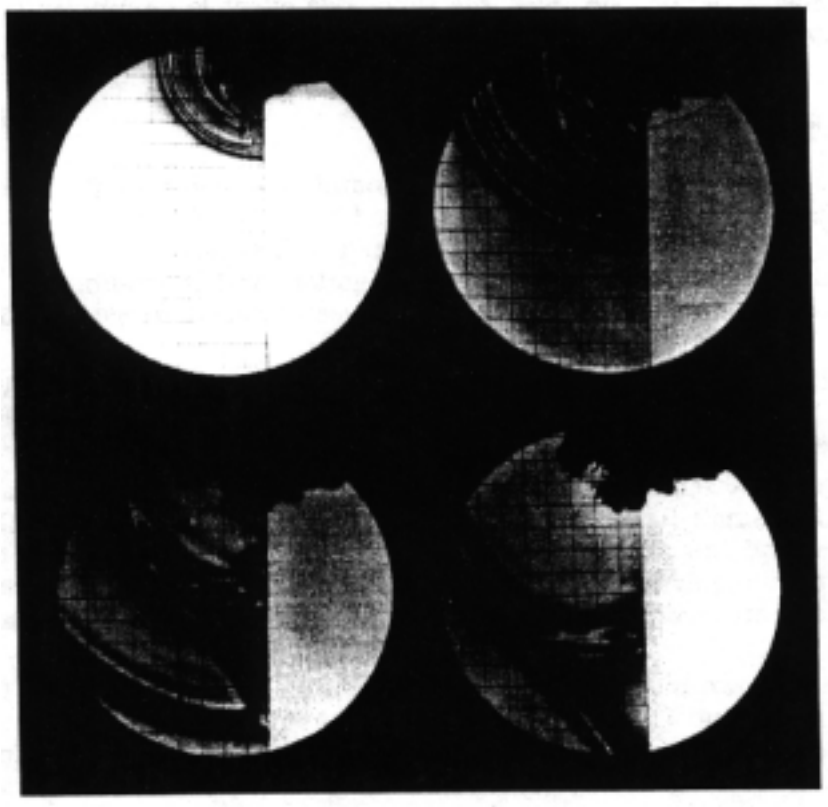

Fig. 6.18. Sequence of isochromatic patterns in semi-infinite plate subject to localized blast load.

For quantitative measurements, careful calibration of model materials at different strain rates is extremely important. In general, the stress-optical coefficient varies with strain rate. Some investigators have found materials that exhibit essentially constant stress-optical coefficients over a great range of strain rates, and other materials that exhibit essentially constant strain-optical coefficients. Use of such materials greatly simplifies calculation of stress or strain fields from relative retardation data.

6.14. PHOTOELASTIC-COATING METHOD

With the concepts of model photoelasticity now well in hand, consideration of the photoelastic-coating method is a simple transition. In this case, the photoelastic material is applied as a thin layer on the surface of an actual structural part. The part if made uniformly reflective — usually by use of a reflective paint or reflective cement—so that light traverses the coating and reflects back for a second traversal of the photoelastic material. The part may be loaded *in situ* in tests of the prototype assembly. This method is particularly useful for

determining stresses on free (unloaded) surfaces of three-dimensional bodies, where the prototype is already available.

An important basic distinction exists between the photoelastic-coating method and model photoelasticity. In the coating method, the actual structural part is analyzed, usually under actual working forces. In contrast, non-metallic models and simulated loading is required in model photoelasticity. Furthermore, the coating method is not restricted to elastic deformation. Correctly chosen coating materials exhibit linear strain-birefringence behavior, regardless of the magnitude and nature of the strains developed in the structure.

A typical optical system is shown schematically in Fig. 6.19. In practice, the obliquity of illumination is small, normally less than 5° and conditions of normal incidence are assumed. Large-field instruments — used to scan and observe fields several inches in diameter — and small-field or microscope-type instruments — used for pointwise measurements — are both usually designed in this fashion. In both cases, the instrument is usually constructed with a rotatable, calibrated analyzer to permit fractional-fringe-order measurements by analyzer rotation.

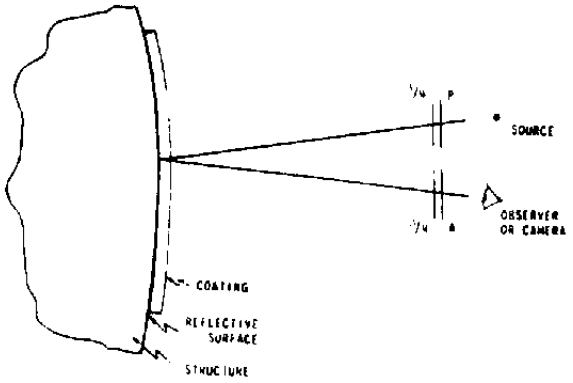

Fig. 6.19. Reflection polariscope arrangement for photoelastic-coating observations.

While the photoelastic effect is one and the same, symbols that have gained wide usage in coating work are different than those already used in this text. The strain-optical relationship is usually written as

$$\varepsilon_1 - \varepsilon_2 = \frac{\delta}{2tK} \tag{6.8}$$

where ε_1 and ε_2 are the principal strains at a point in the coating, $2t$ is the path length through coating, t is coating thickness, δ is the relative retardation, measured in the same units as t, and K is the strain-optical coefficient, a dimensionless quantity.

There is a direct correspondence between stress-optical and strain-optical coefficients for photoelastic materials operating in the linear stress-strain regime, namely

$$f = \frac{E\lambda}{1+\nu}\left(\frac{1}{K}\right)$$

where ν is Poisson's ratio, and λ is the wavelength. Clearly, either coefficient could be used to define the optical effect.

An interesting demonstration of the photoelastic-coating method is shown in Fig. 6.20. The patterns exhibit the optical effect for a notched tensile specimen of aluminum with a 0.070-in. (1.8-mm) coating. In (a) the deformation was elastic, in (b) the maximum strain was a small multiple of the yield strain. and in (c) the aluminum was stressed well into its plastic zone. Upon

unloading, the residual strains resulting from plastic deformation produced the isochromatic pattern shown in (d).

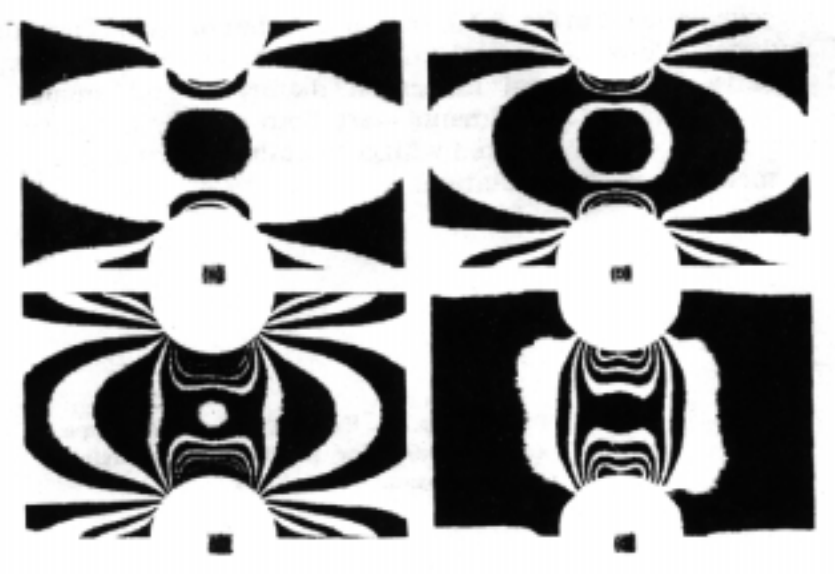

Fig. 6.20. Isochromatic patterns for aluminum tensile bar using photoelastic-coating method: (a) elastic strains: (b) and (c) plastic strains: (d) residual strains.

While peak strain would be expected at the center of the notch boundary for homogeneous plastic materials, the curious double peak occurring at the notch in Fig. 6.20(c) and (d) is presumably caused by anisotropic material properties of the rolled aluminum. A dark-field circular polariscope was used, as evidenced by the black zero-order fringes at the free corners. In this case, background illumination was employed to yield the bright background and sharp definition of boundaries.

Fig. 6.21. Photoelastic-coating analysis large aircraft-landing-gear component.

Figure 6.21 shows an application of the photoelastic-coating method to a critical component of a modern aircraft landing gear. Complete analysis gave the locations, magnitudes, and directions of the maximum principal strains. The thin curved line through the center of the

pattern is a butt joint between two pieces of coating material. Note that the isochromatic fringes cross the joint essentially undisturbed, so large areas can be covered by several smaller sheets of coating material. The contour sheet method was employed to apply the coating to this component.

The contour sheet method is a relatively easy, highly suitable method of coating complex surfaces. It consists of pouring a resin onto a flat, nonsticking surface to cast a sheet of predetermined thickness. When the sheet reaches the gel stage, it is lifted off (Fig. 6.22) and contoured to the shape of the structural part (Fig. 6.23). In gel stage, the plastic is very flexible and formable, and it can be worked into complex shapes with the fingers. Experience shows that resultant variations in thickness of the sheet are quite small. The contoured sheet is allowed to remain on the structural part while its curve is continued. Then the cured coating is removed, a reflective cement is applied, and the coating is bonded to the structure. Figure 6.23 shows a metal part with one section of contoured coating already cemented in place and another section ready for bonding.

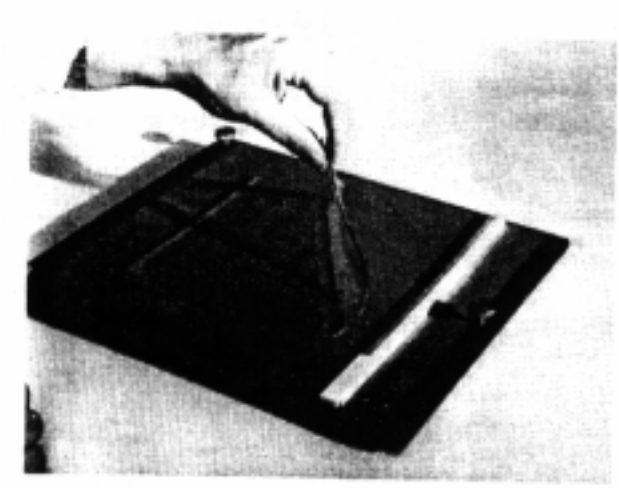

Fig. 6.22. Lifting a partially polymerized sheet of photoelastic- coating material.

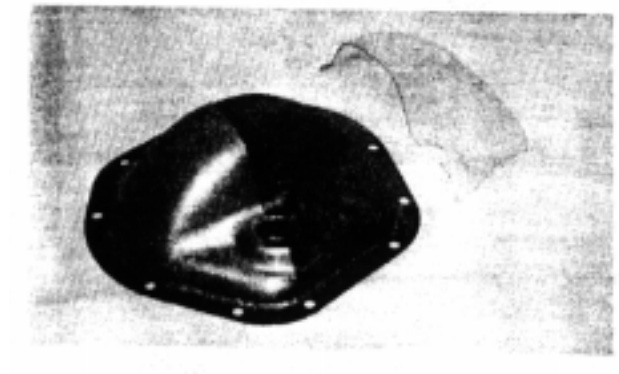

Fig. 6.23. Contoured and cured coating ready for bonding to structural part.

To apply coatings to net surfaces of structures or specimens, fully cured sheets of predetermined thickness are merely bonded in place. Boundary shapes (for example, holes and curved edges) may be cut in the coating either before or after bonding, but the boundary shape of coating and structural component must always be the same.

Discontinuous deformations can be studied with thin coatings. Slip deformation in mild steel is shown in Fig. 6.24 on a microscopic scale. The figure shows an arc of about 1 square millimeter. Very thin coatings, of the order of a few thousandths of an inch, can be used for such observations.

Fig. 6.24. Microscopic view of isochromatic fringes in thin coating, showing slip bands in steel.

In coating analyses, the limiting strain applied to the coating is governed by the limiting strain in the workpiece (i.e., the structural part under investigation). Frequently, this is considerably lower than the elastic-limit strain for the photoelastic material. and we do not take full advantage of the photoelastic sensitivity of the coating. For coatings of the greatest strain-optical sensitivity available today (1977) $K = 0.2$. Table 6.1 shows the isochromatic fringe order, $\overline{N}$, that would be developed in a 1/8-in. (3.18-mm)-thick coating of this sensitivity; the workpiece is a tensile specimen stressed to its elastic limit.

Table 6.1. Fringe-level comparison

Material	Elastic limit, σ_{EL}		Young's modulus, E		ε_{max}	$\overline{N} = \varepsilon_{max} \times (1+\nu)2tK/\lambda$
	(ksi)	(MPa)	(10^6 psi)	(GPa)	($\mu\varepsilon$)	
Structural steel	40	275	30	207	1330	4.0
Aluminum, 2024T4	44	303	10.5	72	4190	12.6
Aluminum, 7075T6	75	517	10.4	72	7200	21.6
Magnesium alloy	30	207	6.5	45	4620	13.9
Concrete	3	21	5.0	35	600	1.8
Wood, pine parallel to grain	4	28	1.5	1.0	2700	8.0

$K = 0.2$; $t = 0.8$; $\lambda = 550$ μm; $\nu = 0.3$. 1 psi = 6.895 kPa; 1 in = 25.4 mm.

We find that 1/8-in. (3.18-mm) coatings on aluminum, magnesium and wood are capable of providing as many fringes as are typically developed in model photoelasticity, and sensitivity is not a limitation. For concrete or structural steel, the fringe orders are lower, and the determination of fractional fringe orders would be called for in quantitative analyses. Similarly, fractional fringe orders would be measured with aluminum, etc., if thinner coatings are employed or if working stresses are well below the elastic limit. Analyzer rotation, compensation and color matching are often employed.

Since sensitivity is proportional to coating thickness, the question of how thick the coating can be made has gained attention. The subject is discussed in the Proceedings of the SESA under titles pertaining to thickness effects in photoelastic coatings. To generalize, one can show that the

strain in the coating exactly matches that at the structure-coating interface when no shear forces, or shear tractions, are developed at the interface [11]. Then, there is no direct limitation on coating thickness.

For structural parts in plane stress, interface tractions are not developed along the entire sandwich — but only near external boundaries of the coating where the coating is forced to take the same displacements as the underlying structure. For example, let a flat tension bar of any irregular boundary shape be mated with a flat coating material of the same shape. If the coating is merely clamped at its end to the tension bar, the two elements will experience identical displacements and strains everywhere, except in the immediate vicinity of the clamps. Even when the coating is bonded along the entire surface, shear tractions are developed only near the ends previously clamped, and no forces are developed in the adhesive in the remainder of the sandwich. The strain is constant through the thickness of the coating and equal to the interface strain. Under these conditions — zero interface tractions — the photoelastic measurement provides an accurate account of the surface strain the structure.

This argument holds exactly when Poisson's ratio of the structure and coating are exactly equal. Since Poisson's ratio is nearly the same for most structural materials and common coating materials, there has been no evidence of significant discrepancies associated with this mismatch.

When the coating is not in a state of plane stress, the coating would not automatically deform in exactly the same manner as the surface of the workpiece. Here, the adhesive develops shear tractions in interior zones to provide the identical displacements at the interface. When shear tractions act on one side of the coating, we find that the strain does not remain constant through the thickness of the coating. The strain obtained from the birefringence measurement is an integrated or average strain, not the interface strain. As the coating is made thinner, the measured strain approaches the actual strain on the surface of the workpiece.

Experience with engineering structures shows that this deviation is seldom of large magnitude. The natural deformation of the coating, subject to its geometry and boundary constraints, is generally very similar to the surface deformation of a body having the same surface shape. The shear tractions are not responsible for the total deformation of the coating, but rather, they introduce the fine adjustment required for identical interface displacements. Shear tractions are then small, and average strain through the coating thickness remains a good approximation of the interface strain.

In the event of any uncertainty, the investigator must establish whether the measured average strains adequately represent the true interface strains. The most convenient test consists of increasing or decreasing the coating thickness by applying an additional coating or by machining down the first coating. If the birefringence per unit-coating thickness remains unchanged, average strains equal interface strains. Otherwise, the analysis must be repeated with a thinner photoelastic coating.

6.15. THREE-DIMENSIONAL PHOTOELASTICITY

Together with the introduction and widespread availability of suitable plastics, we witnessed the development and rapid growth of three-dimensional photoelasticity. This is important not only because so many practical stress problems fall into this category, but also because photoelasticity provides a unique opportunity for determination of stresses inside a body.

Techniques of three-dimensional photoelasticity are based upon another property of certain photoelastic plastics. A model made from such material is heated to its stress-annealing temperature; it is stressed — usually by deadweight loading; and it is cooled slowly with the weights still applied. The loaded model deforms at the elevated temperature, and this *elastic* deformation remains fixed during cooling. At room temperature, the weights are removed, but a mayor portion of the deformation remains locked in the model. Significantly, a photoelastic

pattern corresponding to the elastic state of stress remains fixed in the model together with the deformation.

This is called the *frozen-stress* phenomenon, for the photoelastic pattern is "frozen" into the model during the slow-cooling process. It is a remarkable fact that such models can be cut into any number of elements without disturbing the photoelastic patterns. Accordingly, slabs are normally sawed out of three-dimensional models and analyzed individually in the manner of two-dimensional photoelasticity. The mechanical and optical anisotropy remains permanently fixed in the model, and with suitable materials, isochromatic patterns remain unchanged after several years of storage.

Plastics which exhibit the stress-freezing effect are diphase materials, i.e., they possess two sets of intermolecular bonds, each affected differently by temperature. It is convenient to represent the diphase plastic by an analogous working model. In the analog, these phases are characterized by two separate materials, interspersed in a homogeneous manner. Thus, we can think of an elastic, highly porous sponge with its interstices completely filled with pitch or tar. The pitch behaves as an elastic solid at room temperature, but at the elevated critical or annealing temperature it behaves as a liquid. Thus, at elevated temperature, the primary network of bonds, or the sponge, carries the applied loads, while the secondary network remains unstressed. This state of elastic deformation is then preserved as the pitch hardens, during the cooling or freezing cycle. After the freezing cycle, the loads are removed, but the body does not become stress free. Instead, a system of self-equilibrated stresses is developed in which internal forces exerted at each point by the sponge are balanced by equal and opposite forces exerted by the pitch.

The analogy allows for subsequent slicing of the model, too, for the self-equilibrated stresses are not disturbed when any element is dissected from the body. Thus, no stress relaxation occurs in the slicing operation, and the relative retardations present in the model remain unaltered by the slicing operation.

Figures 6.25 and 6.26 illustrate an application of the frozen-stress technique. A photoelastic model used for a three-dimensional centrifugal stress study is shown in Fig. 6.25. The model was machined from a solid, stress-free slab of epoxy plastic; the entire circular body was produced, but the portion shown here is the part remaining after sections were cut out for analysis. The stress-freezing cycle was carried out in an oven equipped with a firmly mounted motor-driven shaft. The model was mounted on the shaft, the temperature raised to the critical or annealing temperature, high-speed rotation was maintained at constant speed for the entire period of slow cooling to room temperature. Thus, the only forces acting on the model during the stress-freezing cycle were centrifugal forces (plus a trivial amount of aerodynamic drag in this case) and the corresponding centrifugal-stress system could be analyzed.

Fig. 6.25. Photoelastic model for three-dimensional centrifugal-stress study.

It should be noted that slow cooling is required to avoid the introduction of temperature gradients and associated thermal stresses in the model.

Slices or thin slabs were then dissected from the model in regions of interest. This is typically accomplished by sawing out oversize slabs and machining their surfaces on a milling machine or lathe. Alternately, a diamond-impregnated cut-off wheel is used with a copious flow of liquid coolant, usually water. Precautions are taken in machining to avoid heating the part, for otherwise relaxation of frozen stresses and introduction of thermal stresses may occur.

Figure 6.26 shows the isochromatic pattern for a slice taken from this model along its central plane. Stress amplification resulting from the discontinuities in the geometry of the part become clearly evident. Since this is a section taken along a plane of symmetry, two principal stresses at every point lie in this plane. Along the boundaries of the hole and slots, one of these principal stresses is zero, and the other — the tangential stress — is directly proportional to the isochromatic fringe order. Elsewhere, the isochromatic pattern yields the difference of principal stresses lying in the plane of the slice.

Fig. 6.26. Isochromatic pattern for central slice.

In most three-dimensional analyses, the stresses along the surface of the part are of primary interest, since structural failure usually originates at the surface. While several alternatives are possible, a representative analysis of surface stresses proceeds according to Fig. 6.27, as follows:

1. The surface stresses are desired along a line (*s*-*s*). Remove a slice normal to the surface containing the line (Fig. 6.27(b)); observe normal to the slice as shown by the heavy arrow and measure the isochromatic fringe order. At the surface, the fringe order is proportional to the difference of secondary principal stresses,[8] $\sigma_s - \sigma_n$, but since $\sigma_n = 0$, σ_s is determined alone; call this stress *A*. The sign of *A* can be determined readily. If *A* is positive, or tensile, the fringe order will diminish when a compressive force is applied to the slice along *s*-*s*; if compressive, the fringe order will increase.[9] Alternately, the sign can be determined by use of a wedge-type compensator or by analyzer rotation.

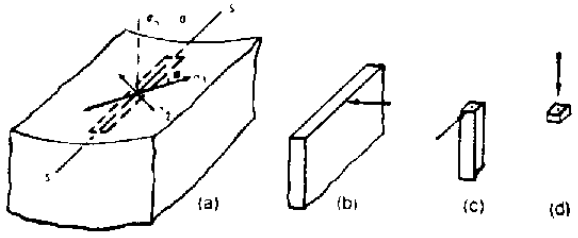

Fig. 6.27. Steps in the analysis of surface stresses along line *s*-*s*.

[8]Secondary principal stresses are, by definition, the largest and smallest normal stresses acting in the plane perpendicular to the direction or incident light (see Chapter 1, Section 1.2).

[9]This is true for epoxies and other stress-freezing model materials commonly used. However, some materials exhibit the opposite behavior wherein birefringence Introduced by frozen tensile stress is diminished by additional tensile stress applied at room temperature. This material characteristic can be determined by a simple test.

2. Subslice and measure the isochromatic fringe order in the perpendicular direction, as indicated in Fig. 6.27(c). As before, the surface stress normal to the direction of observation is determined; ascertain its sign and call this stress *B*.

3. Subslice to obtain a thin element and observe normal to the surface. Measure the angle defining either principal-stress direction with respect to the edges of the element. In addition, the fringe order can be measured and $\sigma_1 - \sigma_2$ calculated for use as a check on individual σ_1 and σ_2 values. Note that the check will not be effective when the stress gradient through the thickness of the final slices is large.

4. Calculate the surface stresses, σ_1 and σ_2 by

$$\sigma_1, \sigma_2 = \frac{A+B}{2} \pm \frac{A-B}{2\cos 2\phi} \tag{6.9}$$

in which the positive sign gives σ_1, and the negative sign gives σ_2. For cases in which the stresses are desired at one surface point only, rather than along a line, a slice parallel to the surface may be taken first for observation of isoclinics. Then the subslices can be made parallel to the directions of principal stress ($\phi = 0°$).

Surface stresses are frequently required along sections of symmetry, and here the technique is much simpler [12]. Steps 1 and 2 are followed as before, but line *s-s* is taken as the line of symmetry. Since $\phi = 0°$, *A* and *B* are the principal stresses and no further measurements or calculations are required. The accuracy is superior to that obtained when principal directions are not known in advance, since the determination does not depend upon measurement of ϕ and the errors inherent in that measurement.

When surface stresses are required at a specific point, or along a succession of points, the *core method* is a practical technique [13]. As illustrated in Fig. 6.28, a cylindrical specimen containing the required surface point is cut from the 3-D photoelastic model. A trepanning or coring tool — essentially a hollow end-milling tool — is used to cut the cylindrical surface; a generous flow of liquid coolant should be used. Then the specimen is cracked off at its base, using a close-fitting tube.

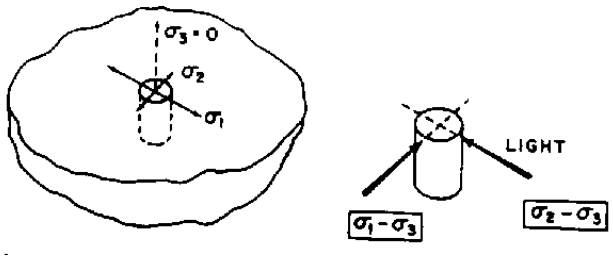

Fig. 6.28. Stress system at the surface of a core specimen.

The cylindrical specimen is observed in a miniature polariscope such as illustrated in Fig. 6.29. A simple immersion tank containing a liquid of refractive index approximately equal to that of the model material is required in order to prevent diffusion and refraction of light be the rough cylindrical surface of the specimen. Use of a compensator is very convenient, since it provides the sign of the stress as well as the fringe order.

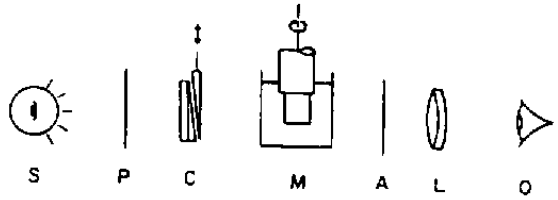

Fig. 6.29. Typical compact optical system for the core method: (S) white-light source; (P) polarizer; (C) compensator; (M) core specimen in immersion cell; (A) analyzer; (L) magnifier or low-power microscope; (O) observer.

The specimen is rotated slowly while fringe order at the surface is observed. Since σ_1 is larger than any secondary principal stress in the surface. and since σ_3 is always zero, the orientation which yields a birefringence proportional to σ_1 is the orientation of maximum birefringence. Thus, the method employs the following simple procedure:

1. Rotate the cylinder to the position of maximum birefringence.
2. Measure the fringe order $\overline{N}_{\max}$ at the free surface for this orientation.
3. Rotate the specimen through 90°.
4. Measure the fringe order $\overline{N}_1$, for this orientation.
5. Calculate $\sigma_1 = f\overline{N}_{\max}/d$ and $\sigma_2 = f\overline{N}_1/d$, where d is the diameter of the specimen. In this context (and only here), σ_1 is the numerically larger principal stress, rather than the algebraically larger.

Figure 6.30 illustrates the isochromatic pattern for a slice taken from a three-dimensional model of a dovetail joint in a turbine rotor. The pattern is somewhat similar to that of Fig. 6.9, but there the stresses are biaxial while here they are triaxial. Again the slice was thin, the 1× pattern exhibited only low birefringence, and fringe multiplication was used to enhance data retrieval. Thin slices are essential in cases where a significant stress gradient exists in the direction perpendicular to the plane of the slice: even where this gradient is small, thinner slices permit the economy of smaller models.

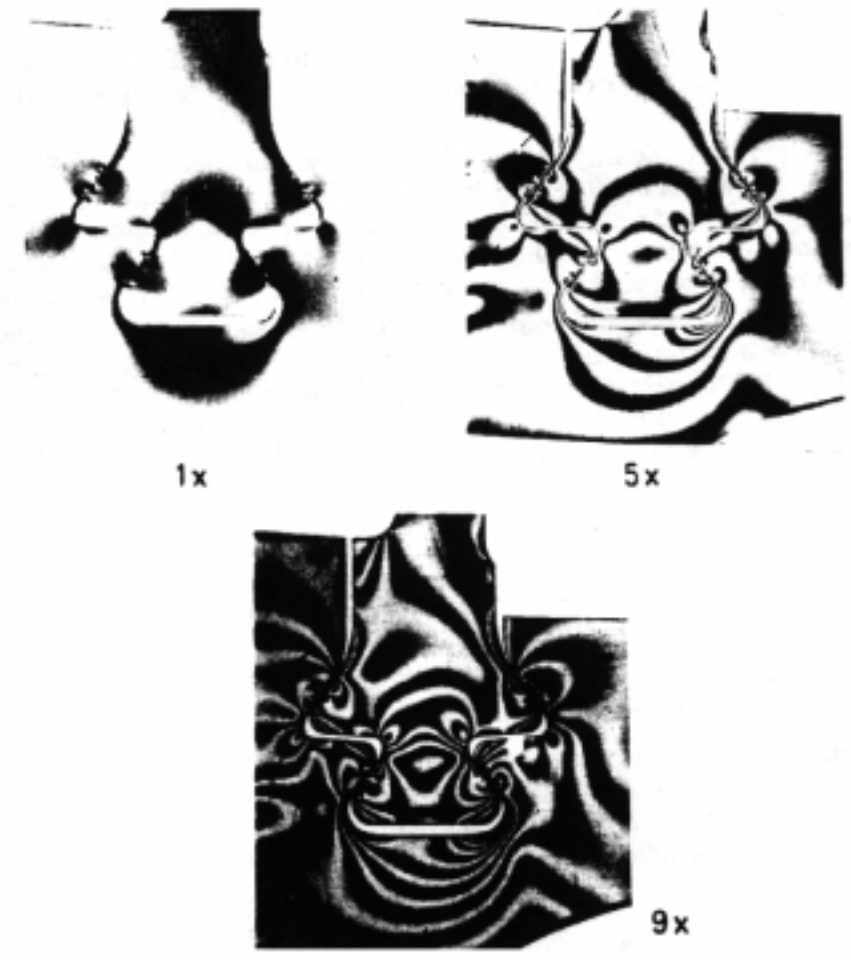

Fig. 6.30. Isochromatic pattern in slice from a three-dimensional model of the blade-attachment section of a jet-engine fan rotor. Multiplication of isochromatic fringes by 1, 5 and 9 was employed.

An interesting feature found here is that only one of the eight dovetail fillets is highly stressed, namely, the lower right fillet. Redesign efforts to reduce this one stress concentration could be handsomely rewarding.

The photoelastic methods already discussed provide the complete state of stress on free (unloaded) surfaces. At interior points, and at loaded surfaces such as the contact zones in Fig. 6.30, photoelastic measurements yield the difference of secondary principal stresses and secondary principal stress directions for any direction of observation. These measurements, taken in any three directions (usually mutually perpendicular), provide sufficient data to determine the true maximum shear stress and Its direction at any point in the body. Similarly, they provide sufficient data to calculate the octahedral shear stress. For those problems in which either of these shear stresses is the criterion for flow or failure, the photoelastic data yields the pertinent stresses.

Three-dimensional problems which require determination of individual stress at interior or loaded boundary points can be solved by means of the three-dimensional problems which require determination of individual stress at interior or loaded boundary points can be solved by means of the three-dimensional shear-difference method [14,15]. As in two-dimensional analysis, supplementary information is required, and it is obtained by utilizing conditions of elasticity theory. By starting at a point of known stress, at a free boundary for example, it is possible to sum every increment of change of stress along any path, and thus calculate the complete state of stress at any interior point.

Epoxy formulations are used almost exclusively today for three-dimensional models [16]. In order to obtain stress-free material, lengthy, carefully controlled thermal curing cycles are employed, extending several weeks for thick sections. Accordingly, models are usually machined from previously stockpiled blanks, although models are sometimes cast to final size. Models are machined with common metalworking tools — lathe, milling machine, drill press, etc. Heating is avoided by use of sharp tools with large rake angles, by high cutting speeds and moderate feeds.

Time-edge effect caused by moisture absorption is again encountered. Moisture is driven out of the model boundaries when exposed to the atmosphere. Since a long time is required to attain uniform moisture content throughout the volume of the model material, investigators usually attempt to maintain zero-moisture content. Parts are kept in a dessicator except when being sliced or viewed in the polariscope. Alternately, moisture can be driven out after the slicing operation by baking at a temperature well below the stress-annealing point.

A permanent edge effect may occur in the stress-freezing process as a result of oxygen absorption, again revealing Itself as sharply curving paths of isochromatics as they approach the edge of a slice. Oxygen is absorbed into the surface of the model at the elevated temperatures of the stress-freezing process, so excess temperature (above the annealing temperature) and excess time at elevated temperature should be avoided. The epoxy formulations that exhibit lower annealing temperatures also exhibit less (to none) of this edge effect. This permanent edge effect can be prevented by performing the stress-freezing operation in an inert atmosphere. A small positive pressure and flow of nitrogen into the stress-freezing oven is a relatively easy and successful technique.

A limitation of the stress-freezing method — an effective value of Poisson's ratio, $\nu = 0.5$ — has already been mentioned in the section on model-prototype similarity. In efforts to circumvent this limitation, methods which do not require stress freezing and slicing are sought, so that the room-temperature value of Poisson's ratio, approximately 0.3, can be used. The scattered-light method offers promise [17]. Here, a plane of light is passed through the photoelastic model, and light scattered out in the perpendicular direction is observed. In principle, the state of stress throughout the model can be determined by passing the light successively through adjacent planes in the model. The scattered-light method has been used successfully for some special problems.

6.16. CONCLUDING REMARKS

Many topics in the theory and practice of photoelasticity have been omitted or treated superficially on the assumption that the reader will fill these voids once he is stimulated by the basic concepts. Textbooks delve deeper into some of the topics covered here; the *Proceedings of the SESA* and *Experimental Mechanics* are a veritable storehouse of information on individual topics on photoelastic equipment, supplies and commercial literature.

Photoelasticity is a fascinating subject that can be studied at vastly different levels. It is a field in which the beginner can obtain important engineering solutions even before he has gained broad understanding of the methods he employs. And still, it is a field that defies clever engineers and scientists to explain completely certain basic phenomena, or to develop techniques that allow broadest exploitation of this valuable tool of stress and strain analysis.

6.17. REFERENCES

6.17.1. Cited References

1. M. M. Frocht, *Photoelasticity* (New York: John Wiley and Sons, **1**, 382 1941).

2. D. Post, Isochromatic fringe sharpening and fringe multiplication in photoelasticity, *Proc. SESA*, **12**(2) (1955).

3. D. Post, Photoelastic-fringe multiplication—for tenfold increase in sensitivity, *Experimental Mechanics*, **10**(8), 305-312 (1970).

4. D. Vassarheli, Contribution to the calculation of stresses from photoelastic values, *Proc. SESA*, **9**(1) (1951).

5. D. C. Drucker, Photoelastic separation of principal stresses by oblique incidence, *J. Appl. Mech., Trans ASME*, **10**(3), A156 (1943); M. M. Frocht, *Photoelasticity*, Vol. II (New York: John Wiley and Sons, 1948), 413-422.

6. D. Post, A new photoelastic interferometer suitable for static and dynamic measurements, *Proc. SESA*, **12**(1) (1955).

7. D. Post, Generic nature of absolute-retardation photoelasticity, *Experimental Mechanics*, **7**(6), 233-241 (1967) and D. Post, Holography and interferometry in photoelasticity, *Experimental Mechanics*, **12**(3), 113- 123 (1972).

8. W. Goldsmith, Dynamic photoelasticity, *Experimental Techniques in Shock and Vibration*, W. J. Worley, ed., *ASME*, 25-54 (1962).

9. A. J. Durelli and W. F. Riley, *Introduction to Photomechanics* (Englewood Cliffs, N.J.: Prentice Hall, Inc., 1965), 336.

10. A. A. Wells and D. Post, The dynamic stress distribution surrounding a running crack—a photoelastic analysis, *Proc. SESA*, **16**(1) (1958).

11. D. Post and F. Zandman, Accuracy of birefringent coating method for coatings of arbitrary thickness, *Experimental Mechanics*, **1**(1), 21-32 (1961);

12. C. E. Taylor and J. W. Schweiker, A three-dimensional photoelastic investigation of stresses near a reinforced opening in a reactor vessel, *Proc. SESA*, **17**(1) (1959).

13. D. Post, The core method, *Experimental Mechanics*, **2**(3), 89-90 (1982).

14. M. M. Frocht and R. Guernsey, Jr., Further work on the general three-dimensional photoelastic problem, *J. Appl. Mech.* **22**, 183-189 (1955).

15. J. W. Dally and W. F. Riley, *Experimental Stress Analysis* (New York: McGraw-Hill, 1978), 374.

16. M. M. Leven, Epoxy resins for photoelastic use, *Photoelasticity*, M. M. Frocht, ed. (New York: Pergamon, 1963).

17. L. S. Srinath and M. M. Frocht, The potentialities of the method of scattered light, *Photoelasticity* , M. M. Frocht, ed., (New York: Pergamon, 1963).

6.17.2. General References

Cumulative Index, *Proc. of the Society for Experimental Stress Analysis, SESA*, Westport, Conn.

E. G. Coker and L.N.G. Filon, *A Treatise on Photoelasticity* (New York: Cambridge University Press, 1931, reprinted 1957).

M. M. Frocht, *Photoelasticity* , **I** and **II**, (New York John Wiley and Sons, 1941 and 1948).

R. B. Heywood, *Designing by Photoelasticity*, (Chapman and Hall, 1952).

H. T. Jessop, and F. C. Harris, *Photoelasticity Principles and Methods* (Mineola, N.Y.: Dover Publications, Inc., 1952).

Proc. of the International Symposium on Photoelasticity, M. M. Frocht, ed. (New York: Pergamon Press, 1963).